ADVANCED MATERIALS
www.advmat.de

Blocking Ion Migration Stabilizes the High Thermoelectric Performance in Cu_2Se Composites

Dongwang Yang, Xianli Su, Jun Li, Hui Bai, Shanyu Wang, Zhi Li, Hao Tang, Kechen Tang, Tingting Luo, Yonggao Yan, Jinsong Wu, Jihui Yang, Qingjie Zhang, Ctirad Uher, Mercouri G. Kanatzidis,* and Xinfeng Tang**

The applications of mixed ionic–electronic conductors are limited due to phase instability under a high direct current and large temperature difference. Here, it is shown that Cu_2Se is stabilized through regulating the behaviors of Cu^+ ions and electrons in a Schottky heterojunction between the Cu_2Se host matrix and in-situ-formed BiCuSeO nanoparticles. The accumulation of Cu^+ ions via an ionic capacitive effect at the Schottky junction under the direct current modifies the space-charge distribution in the electric double layer, which blocks the long-range migration of Cu^+ and produces a drastic reduction of Cu^+ ion migration by nearly two orders of magnitude. Moreover, this heterojunction impedes electrons transferring from BiCuSeO to Cu_2Se, obstructing the reduction reaction of Cu^+ into Cu metal at the interface and hence stabilizes the β-Cu_2Se phase. Furthermore, incorporation of BiCuSeO in Cu_2Se optimizes the carrier concentration and intensifies phonon scattering, contributing to the peak figure of merit ZT value of ≈2.7 at 973 K and high average ZT value of ≈1.5 between 400 and 973 K for the Cu_2Se/BiCuSeO composites. This discovery provides a new avenue for stabilizing mixed ionic–electronic conduction thermoelectrics, and gives fresh insights into controlling ion migration in these ionic-transport-dominated materials.

Thermoelectric (TE) materials allow direct solid-state conversion between heat and electricity via the Seebeck and Peltier effects.[1,2] Compared to other energy conversion technologies, thermoelectricity has unique technical merits, such as high reliability, long life, and the absence of noise or greenhouse emissions, and finds applications in harvesting industrial waste heat, solar energy, ocean or geothermal energy, heat from automobile exhausts, in powering the deep space probes, as well as managing spot-size distributed cooling of electronic devices and household appliances.[3] To date, TE conversion is mainly driven by the development of higher performing, practically stable, and environmentally friendly TE materials. The major scientific and technological challenge is to compete successfully with the established energy conversion technologies and broaden the range of industrial applications of thermoelectricity. The efficiency of a TE material is gauged by its dimensionless figure of merit ZT, defined as $ZT = \alpha^2\sigma T/(\kappa_L+\kappa_e)$, where α, σ, κ_L, κ_e, and T are the Seebeck coefficient, electrical conductivity, lattice thermal conductivity, electronic thermal conductivity, and the absolute temperature, respectively.[1]

Among various classes of TE materials, mixed ionic–electronic conductors, such as $Cu_2Te/Cu_2Se/Cu_2S$,[4–10] Zn_4Sb_3,[11,12] $Ag_2Te/Ag_2Se/Ag_2S$,[13–17] $AgCrSe_2/CuCrSe_2$,[18,19] Ag_8MX_6 (M = Sn, Ge, Si; X = Te, Se, S),[20–22] and Ag_9AlSe_6/Ag_9GaSe_6,[23–25] constitute a unique family.[26] In the mixed conductors, ionic migration coexists with high TE performance in the same temperature regime, indicating an inherent link between the two. In the context of the phonon-glass electron-crystal (PGEC) and hybrid-crystal paradigms of the TE materials research, the mobile ions induce static

Dr. D. Yang, Prof. X. Su, J. Li, H. Bai, Z. Li, H. Tang, K. Tang, T. Luo, Prof. Y. Yan, Prof. J. Wu, Prof. Q. Zhang, Prof. X. Tang
State Key Laboratory of Advanced Technology for Materials Synthesis and Processing
Wuhan University of Technology
Wuhan 430070, China
E-mail: tangxf@whut.edu.cn

Prof. X. Su, Z. Li, Prof. M. G. Kanatzidis
Department of Chemistry
Northwestern University
Evanston, IL 60208, USA
E-mail: m-kanatzidis@northwestern.edu

The ORCID identification number(s) for the author(s) of this article can be found under https://doi.org/10.1002/adma.202003730.

DOI: 10.1002/adma.202003730

H. Bai, T. Luo, Prof. J. Wu
Nanostructure Research Centre
Wuhan University of Technology
Wuhan 430070, China

Dr. S. Wang, Prof. J. Yang
Materials Science and Engineering Department
University of Washington
Seattle, WA 98195, USA
E-mail: jihuiy@uw.edu

Prof. C. Uher
Department of Physics
University of Michigan
Ann Arbor, MI 48109, USA

and dynamic disorders causing strong disruptions of phonon spectra and phonon propagation, and give rise to a "phonon-liquid" behavior.[4] Meanwhile, the nonmobile rigid sublattice constitutes the conduction path for electrons or holes, resulting in an electron-crystal behavior. Attaining high TE performance in mixed ionic–electronic conductors entails a delicate balance among mobile ions, conduction electrons, and lattice phonons. Yet, while the mobile ions play a constructive role in suppressing the lattice thermal conductivity, they also reveal their destructive influence by undermining the stability of the structure under large electric fields or temperature gradients. Given that a large current density and temperature gradient are indispensable for efficient TE power generation and refrigeration, achieving high TE performance while maintaining high structural integrity remains a formidable challenge for applications of mixed conduction thermoelectrics.

Because of their environmental friendliness, low cost of raw materials and high TE performance, Cu_2Se and its derivatives are among the most notable mixed conductor systems. The early studies of Cu_2Se-based compounds date back to the 1960s, when the 3M Corporation developed and patented $Cu_{1.97}Ag_{0.03}Se$ as a potentially promising TE material,[27] the variants of which were tested by other research institutions, including General Atomics Corporation,[28] Teledyne[29] and the NASA's Jet Propulsion Laboratory.[30,31] In recent years, more in-depth and systematic studies have been reported on Cu_2Se with the aim of optimizing its TE performance,[5,6] improving its chemical stability,[32] and developing new synthesis recipes.[7] Still, the high mobility of Cu^+ ions pose a serious risk to the stability of the material under service conditions that involve high voltage and large thermal gradients. The resulting Cu metal precipitates in the samples and the concomitant structural changes lead to a rapid deterioration of the TE performance, which is the reason why research into the TE prospect of Cu_2Se was once abruptly abandoned.[33,34] Currently, researchers are keen to find ways to inhibit the long-range migration of Cu^+ and thus improve the material's stability. According to the recent work by Qiu et al.,[35,36] it is the material-specific chemical potential difference that governs the precipitation of Cu. Consequently, keeping the operational condition of Cu_2Se below a certain voltage threshold seems to be a safe yet passive and ultimately unsatisfactory solution.

Should the long-range migration of Cu^+ ions be actively inhibited and the carrier concentration self-regulated, Cu_2Se-based materials would have not only excellent TE performance but also good phase stability. This would be extremely conducive to the commercial applications of Cu_2Se. In this study, by in situ forming BiCuSeO nanoparticles in Cu_2Se, the Cu^+ ion modulated electric double layer in the space-charge region due to an ionic capacitive effect in the Schottky junction of Cu_2Se/BiCuSeO interface under the direct current effectively blocks the long-range migration of Cu^+ ions throughout the entire sample and hinders the precipitation of Cu metal. This consequently stabilizes the high TE performance of polycrystalline Cu_2Se composites under high electric field and large temperature gradient. In addition, the interdiffusion of Cu vacancies between the Cu_2Se_{1+x} host matrix and BiCuSeO nanophase during the synthesis process efficiently regulates carrier (hole) concentration around the optimal range for a wide series of compositions. Coupled with the enhanced phonon scattering created by the BiCuSeO nanophase, the overall approach solves the dilemma of phase stability and high TE performance.

Stoichiometric amounts of Cu, Se, and Bi_2SeO_2 were mixed and reacted into Cu_2Se_{1+x}/yBiCuSeO (x = 0, 0.005, 0.010, 0.015, 0.020; y = 0, 0.05, 0.1, 0.3, 0.5 mol%) composites by self-propagating high-temperature synthesis (SHS) reactions,[7,37–39] and densified by the plasma activated sintering (PAS). There are two basic control parameters in this work: the Se excess amount "x" (a.k.a. Cu vacancy) and the mole fraction "y" of BiCuSeO. The relative density of the composite sample is about 95% of the theoretical value, 1–2% lower than that of the pristine material. The primary phase of all samples at room temperature was confirmed to be α-Cu_2Se.[40] The presence of the BiCuSeO phase was verified by X-ray diffraction (XRD) measurements in samples with a significant content of BiCuSeO (e.g., y = 0.5 mol%) (Figure S1, Supporting Information), which documented the crucial role of Bi_2SeO_2 in the SHS reaction with Cu and Se to form the BiCuSeO compound.[39]

The as-formed Cu_2Se_{1+x}/yBiCuSeO composites exhibit excellent TE properties (Figures S2–S19, Supporting Information). Incorporation of BiCuSeO in the Cu_2Se matrix improves the TE properties dramatically. The peak ZT values (ZT_{peak}) of a wide range of composites are above 2 at 973 K (Figure S2, Supporting Information). Specifically, the ZT_{peak} values of $Cu_2Se_{1.005}$/0.1 mol% BiCuSeO and $Cu_2Se_{1.020}$/0.3 mol% BiCuSeO at 973 K are 2.7 and 2.6, increased by 50% and 44.4%, respectively, compared to $Cu_2Se_{1.005}$ (ZT_{peak} = 1.8) and $Cu_2Se_{1.020}$ (ZT_{peak} = 1.8) (**Figure 1**a). Meanwhile, the average ZT value (ZT_{avg}) of $Cu_2Se_{1.005}$/0.1 mol% BiCuSeO and $Cu_2Se_{1.020}$/0.3 mol% BiCuSeO in the range of 400–973 K is 1.52 and 1.44, increased by 79% and 118%, respectively, compared to $Cu_2Se_{1.005}$ (ZT_{avg} = 0.85) and $Cu_2Se_{1.020}$ (ZT_{avg} = 0.66).

The repeatability and reproducibility of high ZT values are often an issue. In this work, the electrical conductivity, Seebeck coefficient, thermal conductivity, and calculated ZT curves of the composites are shown to be well repeatable and reproducible (Figures S9, S12, S17, and S18, Supporting Information). In addition, freshly prepared samples $Cu_2Se_{1.005}$/0.1 mol% BiCuSeO and $Cu_2Se_{1.020}$/0.3 mol% BiCuSeO were cross-checked at the University of Michigan (UM, ZEM-3 in Prof. P. F. P. Poudeu's laboratory) and Huazhong University of Science and Technology (HUST, LFA427 in Prof. Junyou Yang's laboratory). The results agree well with ours, within the instrumental errors (Figure 1a, Figure S19, Supporting Information).

With the excellent TE performance confirmed, an important question pertains to the stability of Cu_2Se. To evaluate the stability of the material, measurements of the conductivity of Cu^+ ions and endurance tests under operational conditions of high current density and large temperature difference were performed. A direct-current polarization method with electron-blocking electrodes was utilized to isolate the ionic conduction by filtering electronic conduction. Solid-state Cu|CuBr|Cu_2Se|CuBr|Cu symmetric pseudogalvanic cells with the electron blocking CuBr|Cu electrodes were constructed[41,42] (cf. Figures S20 and S21, Supporting Information). Upon applying a voltage across the composite, keeping the constant current density of ≈160 mA cm^{-2} (i.e., 100 mA DC passing through the sample), the polarization voltage of the pristine

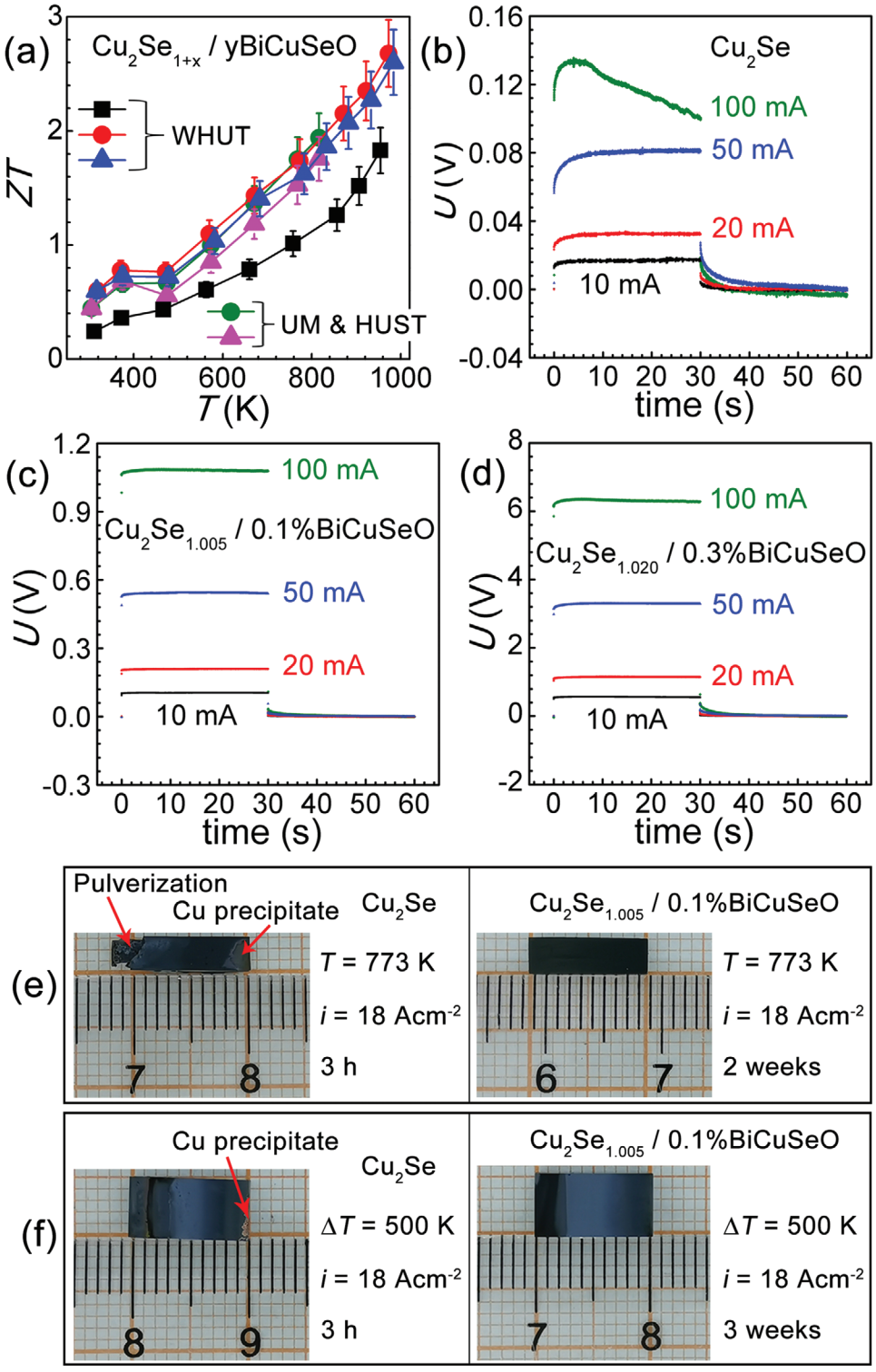

Figure 1. a) Temperature dependence of the *ZT* values of Cu_2Se_{1+x}/yBiCuSeO composites. The squares, circles, and triangles represent Cu_2Se, $Cu_2Se_{1.005}$/0.1 mol% BiCuSeO, and $Cu_2Se_{1.020}$/0.3 mol% BiCuSeO samples, respectively. The black, red, and blue ones indicate testing at Wuhan University of Technology (WHUT) and the brown and pink ones designate cross checking at the University of Michigan (UM, ZEM-3 in Prof. P. F. P. Poudeu's laboratory) and Huazhong University of Science and Technology (HUST, LFA427 in Prof. Junyou Yang's laboratory). b–d) Potential variation curves for: b) Cu_2Se, c) $Cu_2Se_{1.005}$/0.1 mol% BiCuSeO, and d) $Cu_2Se_{1.020}$/0.3 mol% BiCuSeO under different test current at 693 K applied for 30 s. The resulting ionic conductivities at 693 K of Cu_2Se, $Cu_2Se_{1.005}$/0.1 mol% BiCuSeO, and $Cu_2Se_{1.020}$/0.3 mol% BiCuSeO were found to be ≈20, 2.2, and 0.33 S m^{-1}, respectively. e) Comparison between Cu_2Se and $Cu_2Se_{1.005}$/0.1 mol% BiCuSeO when a current of 18 A cm^{-2} was passed through at 773 K. f) Comparison between Cu_2Se and $Cu_2Se_{1.005}$/0.1 mol% BiCuSeO while passing a current of 18 A cm^{-2} through the samples as well as applying a 500 K temperature gradient (*T*-hot ≈ 793 K, and *T*-cold ≈ 293 K).

Cu_2Se starts to drop with time, indicating an increased electrical conductivity and thus Cu-precipitation (Figure 1b). The critical voltage for Cu-precipitation in Cu_2Se is ≈0.1 to 0.14 V, consistent with the previous report.[35] In sharp contrast, upon incorporating BiCuSeO, the stable polarization voltage increases to above 1.0 V for $Cu_2Se_{1.005}$/0.1 mol% BiCuSeO and to 6.0 V for $Cu_2Se_{1.020}$/0.3 mol% BiCuSeO (Figure 1c,d). This indicates that the incorporation of a small amount of BiCuSeO dramatically improves the stability of the Cu_2Se matrix. In addition, based on the DC polarization measurements, the ionic conductivities of Cu_2Se, $Cu_2Se_{1.005}$/0.1 mol% BiCuSeO, and $Cu_2Se_{1.020}$/0.3 mol% BiCuSeO at 693 K were found to be about 20, 2.2, and 0.33 S m^{-1}, respectively (Figure 1b–d, Figure S22, Supporting Information). Evidently, the Cu^+ conductivity in the composites is suppressed by about two orders of magnitude compared to the pristine Cu_2Se, well accounting for their excellent phase stability and reproducibility.

Another evidence of the improved phase stability comes from the shape of a potential variation curve of the pseudogalvanic cell. Cu precipitation is the result of an electrochemical reaction that alters the shape of the potential variation curve. In the absence of Cu precipitation, the potential is almost constant over polarization time. However, with Cu metal precipitating (phase segregation), a notable potential drop over time is observed at a fixed current.[41–43] Clearly, under a 100 mA, the potential across the pristine Cu_2Se decreases gradually with polarization time, indicating the phase instability with Cu precipitation.[41,43] With the presence of BiCuSeO, however, the potential across $Cu_2Se_{1.005}$/0.1% BiCuSeO and $Cu_2Se_{1.020}$/0.3% BiCuSeO samples is not only higher but, more importantly, remains constant upon the same high current of 100 mA. This corroborates the excellent phase stability of the composite under a high current flow.

Moreover, it is well known that the liquid-like nature of Cu^+ ions in the β-phase of the Cu_2Se structure destabilizes the material under sufficiently large current densities and/or temperature differences. Figure 1e,f and Figures S23–S33 (Supporting Information) present the morphology and electrical properties of Cu_2Se, $Cu_2Se_{1.005}$/0.1 mol% BiCuSeO, and $Cu_2Se_{1.020}$/0.3 mol% BiCuSeO composites before and after passing a direct current density of 18 A cm^{-2} at 773 K, or applying a 500 K temperature gradient (with the high-temperature end at 793 K and the low-temperature end at 293 K).

When the current density of 18 A cm^{-2} was passed through a pristine Cu_2Se sample at 773 K for 3 h, serious pulverization and Cu precipitation occurred, and the electrical properties of the damaged sample could not be characterized (Figure S25a, Supporting Information). Under the DC current density of 18 A cm^{-2} and a temperature difference of 500 K across the sample held for 3 h, massive precipitation of Cu, together with a greatly increased electrical conductivity and decreased Seebeck coefficient (Figures S30a and S31, Supporting Information), was observed. This confirms that Cu_2Se is unstable when subjected to large current densities and/or temperature gradients.

The presence of BiCuSeO makes a key difference in the above behavior. For example, the morphology of $Cu_2Se_{1.005}$/0.1 mol% BiCuSeO and $Cu_2Se_{1.020}$/0.3 mol% BiCuSeO samples showed no discernible change after applying 18 A cm^{-2} to the sample for 2 weeks (336 h) at 773 K or imposing a 500 K temperature gradient (Figures S25b,c and S30b,c, Supporting Information). Meanwhile, the electrical conductivity and the Seebeck coefficient measured before and after applying the current and/or the temperature difference returned essentially the same values (Figures S26, S27, S32, and S33, Supporting Information). Hence, a trace amount of BiCuSeO as a secondary phase dramatically improves the phase stability of the composite.

How can such a small amount of well dispersed BiCuSeO nanoparticles be so effective in preventing the migration of Cu^+ ions? In order to reveal the underlying mechanism for this surprising phenomenon, we studied the microstructure and Cu_2Se/BiCuSeO interface in details from different aspects.

Figure 2a,b shows HAADF-STEM images at low magnification and corresponding elemental map (Bi/Cu) of the $Cu_2Se_{1.005}$/0.1mol%BiCuSeO bulk material. Apparently, a large number of uniformly distributed pores with sizes ranging from tens of nanometer to several hundred nanometers are observed. The edge of the pores is rich in Bi, indicating BiCuSeO is mainly attached on their inner wall. Such morphology is strongly related to the formation process of BiCuSeO and is common among mesoporous materials prepared by sacrificial template methods.[44] In an early work, we have demonstrated the crucial role of Bi_2SeO_2 (Figure S34, Supporting Information) in the SHS reaction with Cu, and Se to form the nanosized crystals of BiCuSeO (Figures S35 and S36, Supporting Information)[39] with a polygonal lamellar morphology (Figure S37, Supporting Information). It should be mentioned that no Cu metal precipitate was found inside the nanopores of the Cu_2Se_{1+x}/yBiCuSeO composites before or after the stability measurements under a high current flow or a temperature gradient. Therefore, the uniform distribution of BiCuSeO nanocrystals within the Cu_2Se matrix forms a large number of interfaces which effectively block Cu-ion diffusion. Figure 2c shows the HR-STEM image of the interface between Cu_2Se and BiCuSeO in $Cu_2Se_{1.005}$/0.1mol%BiCuSeO bulk material around the pore. The electron diffraction for Cu_2Se and BiCuSeO indicates that BiCuSeO epitaxially grows on the (131) plane of Cu_2Se coherently, with the [3–10] zone axis of Cu_2Se crystal being parallel to the [22–1] zone axis of the BiCuSeO crystal. As a result, the (002) and (131) planes of Cu_2Se are nearly parallel with (102) and (0–12) planes of BiCuSeO, respectively. This kind of interface would facilitate the formation of Cu^+ modulated electric double layer between Cu_2Se and BiCuSeO, which plays a key role for stabilizing Cu_2Se.

It is well known that both Cu^+ ion and hole carriers in Cu_2Se participant in the electric transport. Thus, understanding the role of Cu^+ ions and the charge transfer at the Cu_2Se/BiCuSeO interface is the key to revealing the underlying mechanism for the enhanced stability. In order to shed light on the charge transfer at the Cu_2Se/BiCuSeO heterojunction, the ultraviolet photoemission spectroscopy (UPS) spectra of Cu_2Se and BiCuSeO compounds were collected, shown in Figure 2d,e, respectively. The work function of Cu_2Se and BiCuSeO are 5.16 and 5.52 eV, respectively. The difference in the work function would drive the hole transfer from BiCuSeO to Cu_2Se, concomitantly forming a depletion layer with the raw built-in electric field in the Cu_2Se/BiCuSeO heterojunction pointing from Cu_2Se to BiCuSeO (Figure 2f). This raw built-in electric field in the Schottky heterojunction is also confirmed by a nonlinear

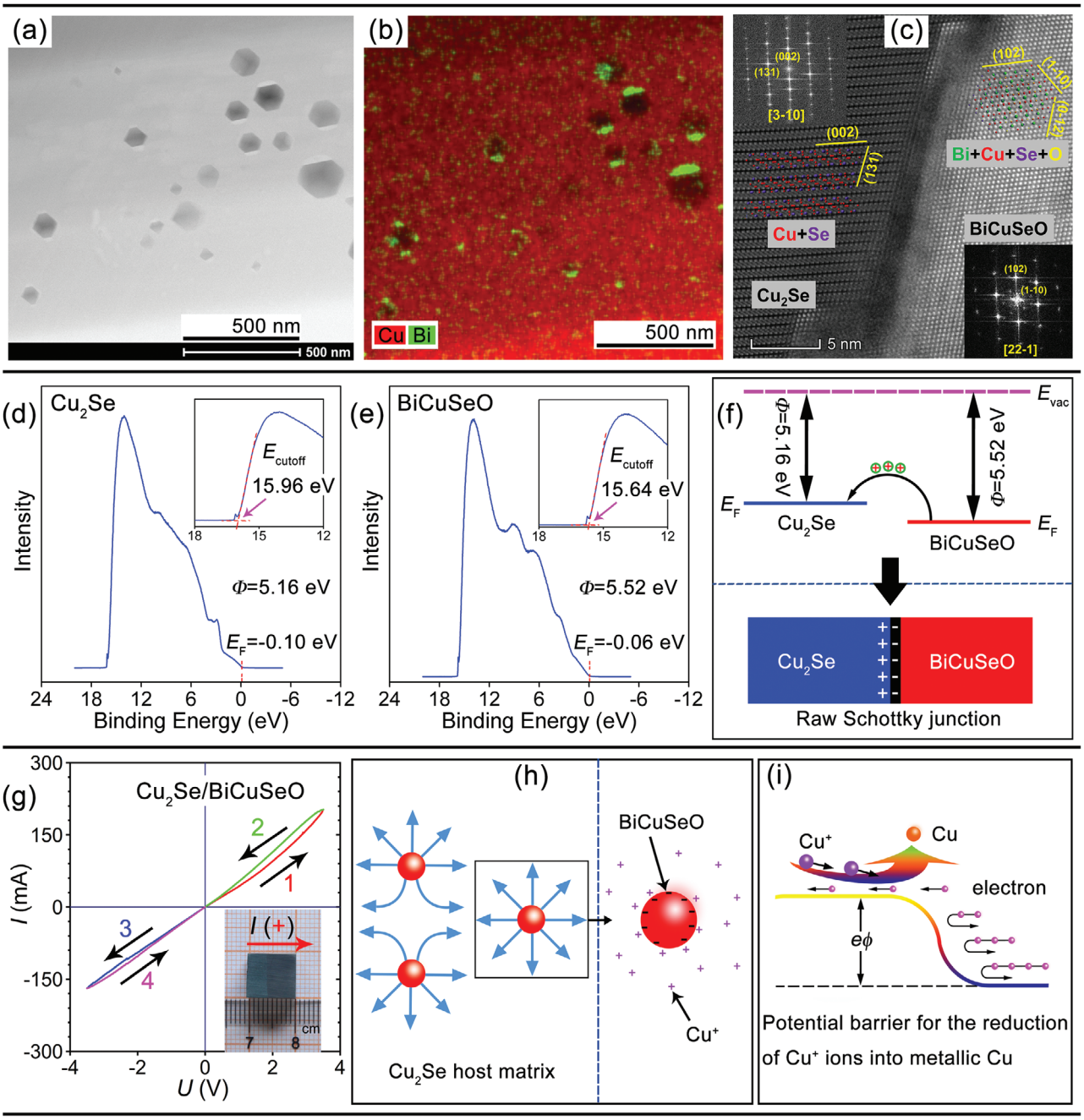

Figure 2. a) HAADF-STEM image at low magnification of $Cu_2Se_{1.005}$/0.1mol%BiCuSeO bulk material, the pores are dark. b) EDS color elemental map (Bi/Cu) of the whole area in (a). c) Interface between Cu_2Se and BiCuSeO around the pore. Orientation relationship: Cu_2Se [3–10]//BiCuSeO [22–1], Cu_2Se (002)//BiCuSeO (102), Cu_2Se (131)//BiCuSeO (0–12). d,e) Ultraviolet photoemission spectrum (UPS) of the Cu_2Se and BiCuSeO. The Fermi edge (E_F) is identified in the diagram, and the secondary electron cutoff edge (E_{cutoff}) is highlighted in the illustration. f) A schematic diagram of hole transfer from BiCuSeO to Cu_2Se driven by the difference in their work functions, and the formation of Cu_2Se-BiCuSeO heterojunction, with the direction of the initial built-in electric field pointing from Cu_2Se to BiCuSeO. g) *I–U* curve of a Cu_2Se/BiCuSeO heterojunction. Clearly, a nonlinear *I–U* curve and hysteresis are observed. h) Schematic illustration of the long range electrostatic field formation and the space-charge distribution in the electric double layer around BiCuSeO in the Cu_2Se_{1+x}/γBiCuSeO composites. A small amount of Cu^+ ions accumulate at the interface between Cu_2Se_{1+x} matrix and BiCuSeO under an external current. This induces interfacial electronic dipole polarization, leading to negatively charged BiCuSeO surfaces. The formed space-charge region in the Cu_2Se and BiCuSeO nanoparticle, where the BiCuSeO nanoparticle is equivalent to a positive point charge due to the capacitive effects of Cu^+ ions. Thus, in spite of a small volume fraction of BiCuSeO, the long-range Coulomb force around BiCuSeO nanoparticles effectively blocks motion of Cu^+ through the sample. i) A schematic diagram of potential barrier in the Schottky heterojunction, which obstructs the reduction reaction from Cu^+ into Cu metal.

feature in the *I–U* curve (Figure 2g) in comparison with a linearly symmetric *I–U* curve of pristine Cu_2Se and pristine BiCuSeO (Figure S39, Supporting Information). This impacts the charge transfer between Cu_2Se and BiCuSeO.

In order to probe the behavior of charge carrier and Cu^+ ions at the heterojunction, forward scan and backward scan of *I–U* curves were measured with the input voltage in the range from −3.5 to 3.5 V. Clearly, under the forward scan the current is smaller than that under the reverse scan, regardless of the current directions, resulting in a hysteretic behavior in the *I–U* curve (Figure 2g). It is well known that the capacitive effect as the Schottky heterojunction can act as a capacitor accumulating charges or Cu^+ ions at the interface due to the potential difference. However, in the case of the electron capacitor, the current under forward scan should be larger than that under the backward scan, which is opposite to experimental observation in the Cu_2Se/BiCuSeO heterojunction. Therefore, the hysteretic gap in the *I–U* curve of the Cu_2Se/BiCuSeO heterojunction is predominantly ascribed to capacitive effects of Cu^+ ions at the interface. The slow reconfiguration process of Cu^+ ion migration is responsible for the hysteresis in the *I–U* curve when the applied voltage is changed. The highly resistive BiCuSeO to the passage of Cu^+ ions, the potential difference between Cu_2Se and BiCuSeO, and the unilateral conductivity of the Schottky junction allow accumulation of mobile Cu^+ ions at the Cu_2Se/BiCuSeO interfaces under the current flowing from Cu_2Se to BiCuSeO. In addition, it is worth noting that due to the unilateral conductivity of the Schottky junction, positive bias voltage allows accumulation of Cu^+ ions at the interface, while the negative bias voltage expels Cu^+ ions from the interface and they migrate and redistribute along the current direction in the host matrix. The difference in the Cu^+ ions concentration in the two sides of the interface region modifies the potential barrier for injection of electronic carrier, leading to the abnormal asymmetry in the *I–U* curve of the Cu_2Se/BiCuSeO heterojunction, which is distinguished from an ideal Schottky junction.

This accumulation of Cu^+ ions at the interface under the direct current induces interfacial electronic dipole polarization, forming a negatively charged surface on BiCuSeO as sketched in Figure 2h. This is accompanied with the formation of an electric double charge layer and an electrostatic field. The formed space-charge region in the Cu_2Se and BiCuSeO nanoparticle, where BiCuSeO nanoparticle is equivalent to a positive point charge due to the capacitive effects of Cu^+ ions, further impedes migration of Cu^+. This agrees well with the much lower Cu^+ conductivity (0.33 vs 20 S m^{-1} for Cu_2Se) and higher critical voltage (>1 vs 0.13 V for Cu_2Se) observed in the Cu_2Se_{1+x}/*y*BiCuSeO nanocomposites. Furthermore, the increase of external voltage difference between Cu_2Se matrix and BiCuSeO nanoparticle, drives more Cu^+ ions to accumulate at the interface, thereby reinforcing the electrostatic field formed in the space-charge region. Thus, in spite of the small volume fraction of BiCuSeO, the Coulomb force around the BiCuSeO nanoparticles effectively blocks long-range motion of Cu^+ through the sample.

Along with the highly mobile Cu^+ ions, Cu metal precipitation at the surface and interface is also a major problem for the stability of Cu_2Se. Practically, Cu metal precipitation is an electrochemical reduction reaction process where the highly mobile Cu^+ ions at the interface or surface close to the upper limit concentration accept electron from the matrix, forming Cu metal.[35] Although the aforementioned Schottky Cu_2Se/BiCuSeO heterojunction facilitates the accumulation of a higher concentration of Cu^+ ions at the interface over that inside of the matrix, the potential difference in the Schottky junction impedes the electron transfer from BiCuSeO to Cu_2Se, unless the energy of electrons is high enough to overcome the potential difference (Figure 2i). Therefore, this special heterojunction obstructs the reduction reaction the Cu^+ ions accumulated at the interface. Thus, incorporation of BiCuSeO not only blocks the long-range migration of Cu^+ ions throughout the sample but it also imposes a potential barrier for the reduction of Cu^+ ion into Cu metal. All these effects contribute to the stabilized Cu-ions in the composite.

To gain more insights into the microscopic nature of ionic migration between Cu_2Se and BiCuSeO, we conducted an in situ transmission electron microscopy (TEM) study. Figure S40 (Supporting Information) shows an HAADF image and EDS mapping results for the Cu_2Se/BiCuSeO heterojunction. As identified by the high resolution image and its corresponding diffraction pattern (Figure S40, Supporting Information), the crystal on the left of the heterojunction is Cu_2Se, while the one on the right is BiCuSeO. When the current flows from BiCuSeO to Cu_2Se (corresponding to the formation of Cu aggregates at the contact point), the critical voltage (threshold) for deposition of Cu metal is 1.1 V (**Figure 3**a). However, when the current flows in the opposite direction from Cu_2Se to BiCuSeO (corresponding to the disappearance of Cu aggregates at the contact point), the critical voltage for rapid Cu^+ migration is 2.3 V (Figure 3b). Moreover, no Cu deposition is observed at the Cu_2Se/BiCuSeO interface despite the fact that the applied reverse voltage is much higher than the forward voltage. Obviously, when the current flows from Cu_2Se to BiCuSeO, the electrostatic field formed by the accumulated Cu^+ ions will oppose migration of Cu^+ from the Cu_2Se matrix and the Schottky heterojunction of Cu_2Se/BiCuSeO increases the potential barrier for electron transfer from BiCuSeO to Cu_2Se. Hence, the critical voltage for rapid migration of Cu^+ ions is significantly increased and no Cu deposition is detected. This further corroborates the Cu^+ ion blocking mechanism in Cu_2Se_{1+x}/*y*BiCuSeO composites and the presence of an additional electrostatic field under the current.

Obviously, the Cu^+ modulated electric double layer in the space-charge region between the Cu_2Se and BiCuSeO phases blocks the long-range ion migration in the entire sample. Along with the Schottky junction, which prevents electron transfer from BiCuSeO to Cu_2Se and thus hinders the reduction reaction, the high TE performance of the Cu_2Se/BiCuSeO composites is stabilized. Additionally, the TE performance of Cu_2Se/BiCuSeO composites is strongly related to its carrier concentration that is determined by the Cu content, i.e., Cu vacancies in the Cu_2Se host. We now discuss the mechanism for modulation of the carrier concentration.

The regulating behavior of the Cu/Se content in the host matrix is confirmed by DSC tests performed on the as-prepared composites (**Figure 4**a and Figure S41, Supporting

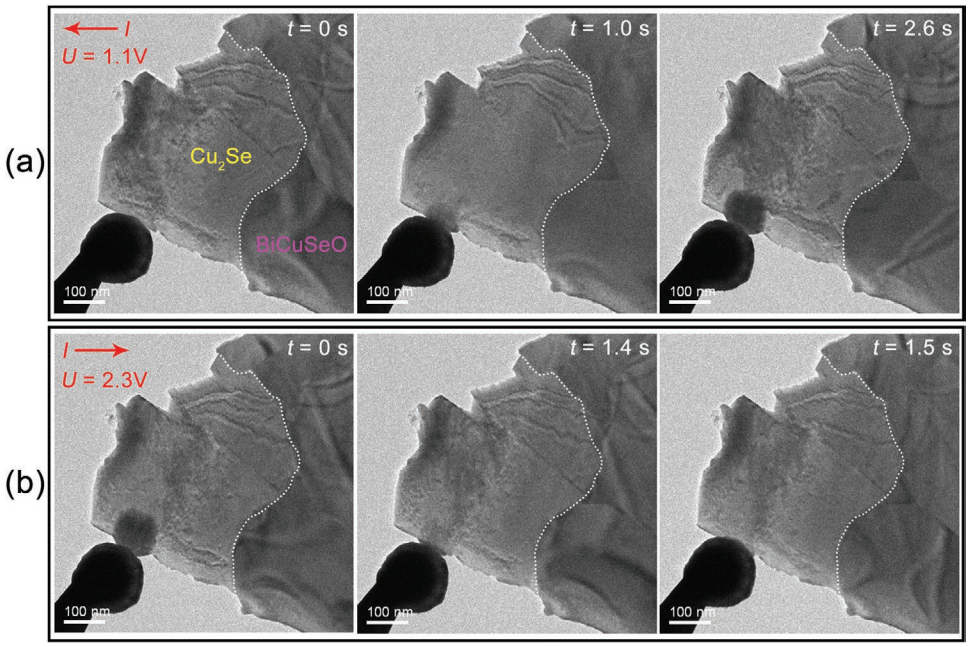

Figure 3. In situ TEM images. a) Different stages (in time) during the current flow from BiCuSeO to Cu_2Se. The developing black spot in the vicinity of the contact is the precipitated copper, which is observed when the applied voltage reaches the critical value of 1.1 V. b) Different stages following the current reversal (the current now flows from Cu_2Se to BiCuSeO). In this case, the critical voltage for rapid migration of Cu^+ (i.e., the disappearance of the previously precipitated copper) is 2.3 V.

Information). For Cu_2Se_{1+x}, the phase transition temperature (T_{tr}) decreases from 399.2 to 387.4 K as the content of Se increases. For Cu_2Se/yBiCuSeO, $Cu_2Se_{1.005}/y$BiCuSeO, and $Cu_2Se_{1.010}/y$BiCuSeO, the T_{tr} tends to shift to a lower temperature, indicating the decreased Cu/Se ratio in the matrix according to the binary Cu-Se phase diagram.[45] For $Cu_2Se_{1.015}/y$BiCuSeO and $Cu_2Se_{1.020}/y$BiCuSeO, T_{tr} tends to shift to a higher temperature, implying an increased Cu/Se ratio in the matrix. The DSC results indicate that the presence of Cu^+ vacancies interdiffusion process during the preparation of Cu_2Se/BiCuSeO composite can modulate the copper content in the host matrix. This helps to maintain the carrier concentration at the optimal region over a wide range of compositions, which is very important for the reproducible synthesis of materials on a large scale.

To reveal and substantiate the mechanism underlying the high TE performance of these composites, low temperature and high temperature transport properties were studied (Figures S4, S6, S8, S11, S14, S16, S42, and S43, Supporting Information). Specifically, Figure 4b shows the relation between the carrier concentration and the composition (x, y) at 600 K. As shown, the optimal carrier concentrations are in the range of (1.0–1.5) $\times 10^{21}$ cm^{-3}, which yields peak ZT values exceeding 2.0. To more clearly see the self-regulation of the carrier concentration by BiCuSeO and Se excess, we present a baseline (red dotted line) derived by assuming that each excess Se atom donates two holes to the composite. Apparently, the presence of BiCuSeO tends to increase (decrease) the carrier concentration when $x \leq 0.01$ (when $x > 0.01$). Since the carrier concentration is positively related to the x-value, the presence of BiCuSeO thus self-regulates the carrier concentration. The pivotal (balance) point is near $x = 0.01$, where the carrier concentration is around 1.0×10^{21} cm^{-3}, close to the lower end of the optimal carrier concentration. It remains an open question how this optimized carrier concentration is achieved over such a wide range of compositions and how it is coordinated with the effectively regulating behavior of Cu vacancies between Cu_2Se and BiCuSeO during the preparation process.

The origin of charge carriers (holes) in Cu_2Se and BiCuSeO is Cu vacancies.[4,46] Actually, the carrier concentration of Cu_2Se is about 4×10^{20} cm^{-3} due to the Cu vacancies and that of BiCuSeO is about 2×10^{17} cm^{-3} at room temperature.[4,7,39] Therefore, driven by the Cu vacancy potential difference, Cu vacancies naturally diffuses from BiCuSeO to Cu_2Se in the Cu_2Se_{1+x}/yBiCuSeO composite when $x \leq 0.01$, and then diffuses from Cu_2Se to BiCuSeO when $x \geq 0.01$. This points to the effective regulation of the relative copper content in the host matrix.

The remarkable reduction of the already low thermal conductivity of Cu_2Se in the composite samples is a contributing factor to the high TE performance. As noticed, the Cu_2Se_{1+x}/yBiCuSeO nanocomposites exhibits low thermal conductivity (Figure 4c), especially at some particular compositions, e.g., $Cu_2Se_{1.005}$/0.1 mol% BiCuSeO (Figure S7, Supporting Information), $Cu_2Se_{1.010}$/0.3 mol% BiCuSeO (Figure S10, Supporting Information), $Cu_2Se_{1.015}$/0.1 mol% BiCuSeO (Figure S13, Supporting Information), $Cu_2Se_{1.020}$/0.1 mol% BiCuSeO, and $Cu_2Se_{1.02}$/0.3 mol% BiCuSeO (Figure S15, Supporting Information). It should be noted that the low thermal conductivity was cross-checked by other group (HUST).

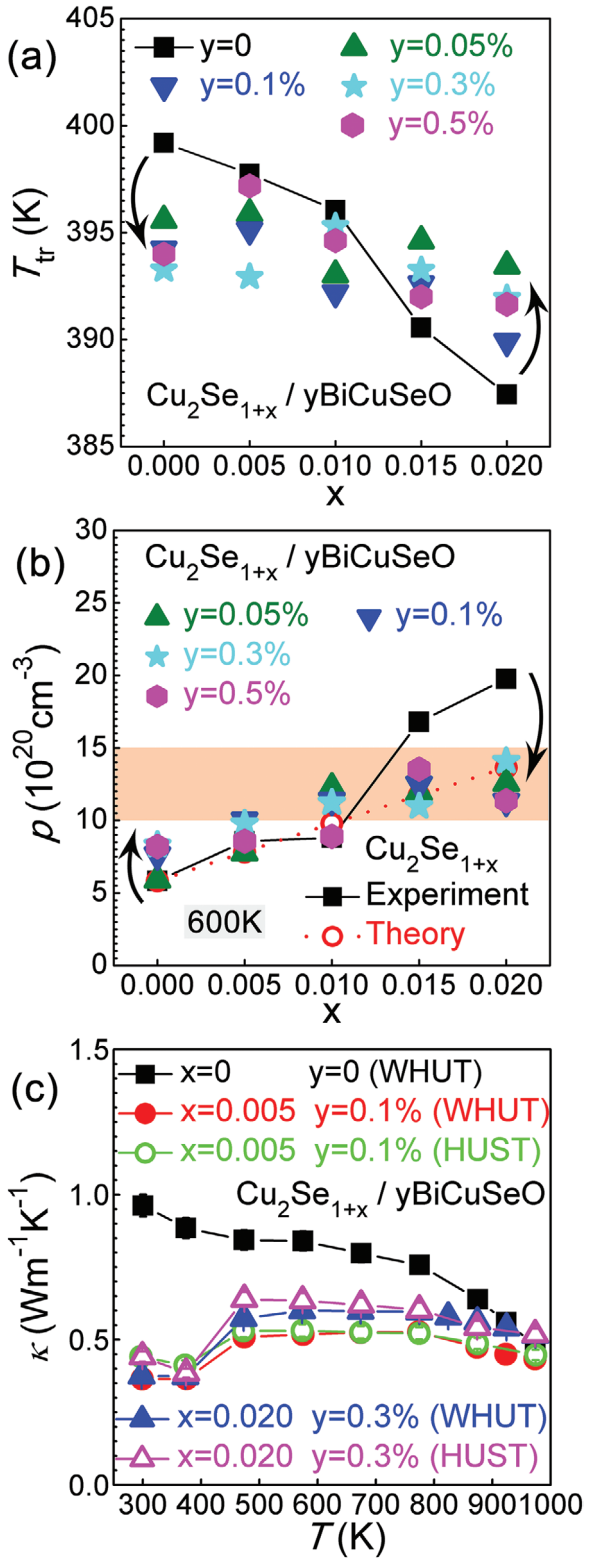

Figure 4. a) Relationship between the phase transition temperature and composition of composite structures. b) Relationship between the carrier concentration (p) of holes and composition of composite structures. The orange region corresponds to the optimal carrier concentration, which yields ZT values exceeding 2.0. Clearly, the incorporation of BiCuSeO can adjust the relative content of copper in the Cu_2Se matrix (as seen in the variation of the phase transition temperature), which, in turn, adjusts the carrier concentration to optimal in a wide range of compositions. c) Temperature dependence of the total thermal conductivity (κ) of Cu_2Se_{1+x}/yBiCuSeO composites. Squares, circles, and triangles represent Cu_2Se, $Cu_2Se_{1.005}$/0.1 mol% BiCuSeO, and $Cu_2Se_{1.020}$/0.3 mol% BiCuSeO samples, respectively. The solid symbols indicate testing at the Wuhan University of Technology (WHUT) while the open symbols designate cross checking at Huazhong University of Science and Technology (HUST, LFA427 in Prof. Junyou Yang's laboratory).

The exact origin of the ultralow thermal conductivity in Cu_2Se, however, has been the subject of debate. Several different theories have been proposed. For example, some investigations show that the liquid-like diffusion of Cu^+ ions suppresses the transverse phonons, leading to a dramatically reduced thermal conductivity. They conclude that the higher the ionic conductivity, the lower the thermal conductivity. In contrast, other investigations show that migration of Cu^+ ions cannot prevent the propagation of transverse acoustical phonons, and argue that the lattice anharmonicity, correlated with the diffusion of Cu^+ (diffusion rate and hopping time), is the main origin of the low thermal conductivity.[47] In the context of our experimental data, the decrease in the ionic migration in the samples upon incorporating BiCuSeO nanoparticles is unequivocal. This modified process of dynamic Cu^+ ions may intensify phonon scattering, suppressing the lattice thermal conductivity.[47,48] Moreover, BiCuSeO nanoparticles and nanopores enhance interfacial phonon scattering and strongly scatter the heat-carrying phonons, resulting in an additional reduction of the thermal conductivity and thus high ZT in Cu_2Se_{1+x}/yBiCuSeO composites.

Through an in situ incorporation of nanoparticles of BiCuSeO, the superionic nature of Cu_2Se in macroscopic samples was largely eliminated while maintaining excellent TE properties. The superior phase and physical property stability is realized by creating an ion-modulated interfacial electrostatic field under the direct current that blocks the long-range migration of Cu^+ ions across Cu_2Se_{1+x}/BiCuSeO interfaces and prevents the reduction reaction from Cu^+ to Cu metal. Meanwhile, the effective regulation of the relative content of copper and the concentration of holes in the host matrix through interdiffusion of Cu vacancies between the Cu_2Se_{1+x} host matrix and the BiCuSeO nanophase during the synthesis process maintains high power factor and the carrier concentration at the optimal carrier concentration range over a wide temperature and composition region. These effects stabilize the excellent TE performance under high current/voltage and/or large temperature gradient. Moreover, the lattice phonons are strongly scattered by BiCuSeO nanoparticles and nanopores, dramatically reducing the lattice thermal conductivity. Owing to the optimal hole concentration and the dramatically suppressed thermal conductivity, the Cu_2Se_{1+x}/yBiCuSeO composites attain high peak ZTs of ≈2.7 at 973 K, and the corresponding average ZT values between 400 and 973 K reach a high value of 1.5. The excellent repeatability and reproducibility of TE properties strongly substantiate the proposed mechanism. The results highlight a new strategy for the active control of ion migration and may have broader implications for the stabilization of other systems such as halide perovskites and solid state interfacial behavior in solid state batteries and fuel cells.

Supporting Information

Supporting Information is available from the Wiley Online Library or from the author. Video S1: 3D reconstruction for a pit of $Cu_2Se_{1.005}$/0.1%BiCuSeO composite; Video S2: In situ transmission electron microscopy.

Acknowledgements

The authors acknowledge support from the National Key Research and Development Program of China (2019YFA0704900), the Natural Science Foundation of China (Grant Nos. 51972256, 51632006, 51521001, and 51872219), and the 111 Project of China (Grant No. B07040). D.Y. is grateful to Prof. Wenyu Zhao and Mr. Shifang Ma for their help with high-temperature Hall coefficient measurement at State Key Laboratory of Advanced Technology for Materials Synthesis and Processing in Wuhan University of Technology, to Prof. P. F. P. Poudeu and Mr. Ruiming Lu for cross-checking with high-temperature electrical properties measurement in the University of Michigan, to Prof. Junyou Yang and Mr. Jiwu Xin for cross-checking with high-temperature thermal properties measurement in Huazhong University of Science and Technology, to Prof. Jianbo Wang and Mr. Yuanlin Zhuang for their help with thinning of in situ electron microscopy samples by focused ion beam (FIB) in Wuhan University, to Dr. De Fang for help with UPS measurement in Materials Research and Test Center of Wuhan University of Technology. The S/TEM work was performed at the Nanostructure Research Center (NRC), which is supported by the Fundamental Research Funds for the Central Universities (WUT: 2019III012GX, 2020III002GX), the State Key Laboratory of Advanced Technology for Materials Synthesis and Processing, and the State Key Laboratory of Silicate Materials for Architectures (all of the laboratories are at Wuhan University of Technology). Work at Northwestern University was supported by the Department of Energy, Office of Science Basic Energy Sciences under grant DE-SC0014520, DOE Office of Science (sample preparation, synthesis, XRD, TE measurements). J.Y. acknowledges the support by the Inamori Foundation.

Conflict of Interest

The authors declare no conflict of interest.

Author Contributions

D.Y. and X.S. contributed equally to this work. All authors have given approval to the final version of the manuscript.

Keywords

Cu_2Se, mixed ionic–electronic conductors, Schottky junction, stable thermoelectric materials, thermoelectric properties

Received: May 31, 2020
Revised: July 31, 2020
Published online: September 2, 2020

[1] D. M. Rowe, *CRC Handbook of Thermoelectrics*, CRC Press, Boca Raton, FL, USA **1995**.
[2] H. J. Goldsmid, *Introduction to Thermoelectricity*, Springer, Berlin, Germany **2010**.
[3] J. He, T. M. Tritt, *Science* **2017**, *357*, 1369.
[4] H. L. Liu, X. Shi, F. F. Xu, L. L. Zhang, W. Q. Zhang, L. D. Chen, Q. Li, C. Uher, T. Day, G. J. Snyder, *Nat. Mater.* **2012**, *11*, 422.
[5] R. Nunna, P. F. Qiu, M. J. Yin, H. Y. Chen, L. D. Chen, *Energy Environ. Sci.* **2017**, *10*, 1928.
[6] A. A. Olvera, N. A. Moroz, P. Sahoo, P. Ren, T. P. Bailey, A. A. Page, C. Uher, P. F. P. Poudeu, *Energy Environ. Sci.* **2017**, *10*, 1668.
[7] X. L. Su, F. Fu, Y. G. Yan, G. Zheng, T. Liang, Q. Zhang, X. Cheng, D. W. Yang, H. Chi, X. F. Tang, Q. J. Zhang, C. Uher, *Nat. Commun.* **2014**, *5*, 4908.
[8] Y. He, T. Day, T. S. Zhang, H. L. Liu, X. Shi, L. D. Chen, G. J. Snyder, *Adv. Mater.* **2014**, *26*, 3974.
[9] Y. He, P. Lu, X. Shi, F. F. Xu, T. S. Zhang, G. J. Snyder, C. Uher, L. D. Chen, *Adv. Mater.* **2015**, *27*, 3639.
[10] X. X. Xiao, W. J. Xie, X. F. Tang, Q. J. Zhang, *Chin. Phys. B* **2011**, *20*, 340.
[11] G. J. Snyder, M. Christensen, E. Nishibori, T. Caillat, B. B. Iversen, *Nat. Mater.* **2004**, *3*, 458.
[12] T. Caillat, J. P. Fleurial, A. Borshchevsky, *J. Phys. Chem. Solids* **1997**, *58*, 1119.
[13] M. Ferhat, J. Nagao, *J. Appl. Phys.* **2000**, *88*, 813.
[14] Y. F. Ding, Y. Qiu, K. F. Cai, Q. Yao, S. Chen, L. D. Chen, J. Q. He, *Nat. Commun.* **2019**, *10*, 841.
[15] Y. Z. Pei, N. A. Heinz, G. J. Snyder, *J. Mater. Chem.* **2011**, *21*, 18256.
[16] D. W. Yang, X. L. Su, F. C. Meng, S. Wang, Y. G. Yan, J. H. Yang, J. He, Q. J. Zhang, C. Uher, M. G. Kanatzidis, X. F. Tang, *J. Mater. Chem. A* **2017**, *5*, 23243.
[17] X. Shi, H. Y. Chen, F. Hao, R. H. Liu, T. Wang, P. F. Qiu, U. Burkhardt, Y. Grin, L. Chen, *Nat. Mater.* **2018**, *17*, 421.
[18] B. Li, H. Wang, Y. Kawakita, Q. Zhang, M. Feygenson, H. L. Yu, D. Wu, K. Ohara, T. Kikuchi, K. Shibata, T. Yamada, X. K. Ning, Y. Chen, J. Q. He, D. Vaknin, R. Q. Wu, K. J. Nakajima, M. G. Kanatzidis, *Nat. Mater.* **2018**, *17*, 226.
[19] J. L. Niedziela, D. Bansal, A. F. May, J. X. Ding, T. Lanigan-Atkins, G. Ehlers, D. L. Abernathy, A. Said, O. Delaire, *Nat. Phys.* **2019**, *15*, 73.
[20] W. Li, S. Q. Lin, B. H. Ge, J. Yang, W. Q. Zhang, Y. Z. Pei, *Adv. Sci.* **2016**, *3*, 1600196.
[21] W. F. Kuhs, R. Nitsche, K. Scheunemann, *Mater. Res. Bull.* **1979**, *14*, 241.
[22] X. Shen, C. C. Yang, Y. M. Liu, G. W. Wang, H. Tan, Y. H. Tung, G. Y. Wang, X. Lu, J. He, X. Y. Zhou, *ACS Appl. Mater. Interfaces* **2019**, *11*, 2168.
[23] W. Li, S. Q. Lin, M. Weiss, Z. W. Chen, J. Li, Y. D. Xu, W. G. Zeier, Y. Z. Pei, *Adv. Energy Mater.* **2018**, *8*, 1800030.
[24] S. Q. Lin, W. Li, S. Li, X. Zhang, Z. Chen, Y. Xu, Y. Chen, Y. Pei, *Joule* **2017**, *1*, 816.
[25] B. Jiang, P. Qiu, H. Chen, Q. Zhang, K. Zhao, D. Ren, X. Shi, L. Chen, *Chem. Commun.* **2017**, *53*, 11658.
[26] T. P. Bailey, C. Uher, *Curr. Opin. Green Sustainable Chem.* **2017**, *4*, 58.
[27] E. F. J. Hampl, *Thermoelectric Materials Evaluation Program, Quarterly Technical Task Report No. 46 1976*, U. S. Department of Energy **1976**, https://doi.org/10.2172/5311720.
[28] N. B. Elsner, J. Chin, *Radioisotope Space Power Generator, Annual Report for the Period July 1, 1973 - June 30, 1974 (Report No. GA-A-13426)*, General Atomic Co., San Diego, California, USA **1975**, https://doi.org/10.2172/4178631.
[29] T. E. Hammel, *Selenide Isotope Generator for the Galileo Mission, Program Final Report*, **1978**, https://doi.org/10.2172/5928964.
[30] G. Stapfer, V. C. Truscello, *Development of the Data Base for a Degradation Model of a Selenide RTG (Report No.19770066000)*, NASA JPL, **1977**.
[31] G. Stapfer, *Copper–Selenide System, P-type TPM-217 (Report No. DOE/ET/33003-T5)*, NASA JPL, **1977**.
[32] T. P. Bailey, H. Si, H. Y. Xie, A. Olvera, P. F. P. Poudeu, X. F. Tang, C. Uher, *J. Mater. Chem. A* **2016**, *4*, 17225.

[33] G. Dennler, R. Chmielowski, S. Jacob, F. Capet, P. Roussel, S. Zastrow, K. Nielsch, I. Opahle, G. K. H. Madsen, *Adv. Energy Mater.* **2014**, *4*, 1301581.
[34] D. R. Brown, T. Day, T. Caillat, G. J. Snyder, *J. Electron. Mater.* **2013**, *42*, 2014.
[35] P. F. Qiu, M. T. Agne, Y. Y. Liu, Y. Q. Zhu, H. Y. Chen, T. Mao, J. Yang, W. Q. Zhang, S. M. Haile, W. G. Zeier, J. Janek, C. Uher, X. Shi, L. D. Chen, G. J. Snyder, *Nat. Commun.* **2018**, *9*, 2910.
[36] P. F. Qiu, T. Mao, Z. F. Huang, X. G. Xia, J. C. Liao, M. T. Agne, M. Gu, Q. H. Zhang, D. D. Ren, S. Q. Bai, X. Shi, G. J. Snyder, L. D. Chen, *Joule* **2019**, *3*, 1538.
[37] A. G. Merzhanov, *Arch. Combust.* **1981**, *1*, 23.
[38] A. G. Merzhanov, *Combust. Sci. Technol.* **1994**, *98*, 307.
[39] D. W. Yang, X. L. Su, Y. G. Yan, T. Z. Hu, H. Y. Xie, J. He, C. Uher, M. G. Kanatzidis, X. F. Tang, *Chem. Mater.* **2016**, *28*, 4628.
[40] W. J. Qiu, P. Lu, X. Yuan, F. F. Xu, L. H. Wu, X. Z. Ke, H. L. Liu, J. Yang, X. Shi, L. D. Chen, J. H. Yang, W. Q. Zhnag, *J. Chem. Phys.* **2016**, *144*, 194502.
[41] I. Yokota, *J. Phys. Soc. Jpn.* **1953**, *8*, 595.
[42] I. Yokota, *J. Phys. Soc. Jpn.* **1961**, *16*, 2213.
[43] Y. Y. Liu, P. F. Qiu, H. Y. Chen, R. Chen, X. Shi, L. D. Chen, *J. Inorg. Mater.* **2017**, *32*, 1337.
[44] M. Oschatz, J. T. Lee, H. Kim, W. Nickel, L. Borchardt, W. I. Cho, C. Ziegler, S. Kaskel, G. Yushin, *J. Mater. Chem.* **2014**, *2*, 17649.
[45] V. M. Glazov, A. S. Pashinkin, V. A. Fedorov, *Inorg. Mater.* **2000**, *36*, 641.
[46] L. D. Zhao, J. Q. He, D. Berardan, Y. H. Lin, J. F. Li, C. W. Nan, N. Dragoe, *Energy Environ. Sci.* **2014**, *7*, 2900.
[47] D. J. Voneshen, H. C. Walker, K. Refson, J. P. Goff, *Phys. Rev. Lett.* **2017**, *118*, 145901.
[48] X. Liang, *Appl. Phys. Lett.* **2017**, *111*, 133902.